Tellus (1995), 47A, 815–833
Printed in Belgium – all rights reserved

TELLUS
ISSN 0280–6495

A numerical investigation of surface-induced mesocyclogenesis near the Gulf Stream

By JOSEPH J. CIONE* and SETHU RAMAN, *Department of Marine Earth and Atmospheric Sciences, North Carolina State University, Raleigh, NC 27695-8208, USA*

(Manuscript received 14 September 1994; in final form 20 April 1995)

ABSTRACT

A series of numerical experiments designed to simulate the initial development stages of low-level coastal mesocyclogenesis near the Gulf Stream was recently conducted. Under initially quiescent conditions, surface cyclogenesis in the control simulation occurs along a Gulf Stream meander in a region where the gradients in sea surface temperature (SST) are maximized. A low-level mesovortex on the order of 140 km forms approximately 12 h into the simulation and continues to intensify through 42 h. During the 24–48 h time period, a mesoscale frontal feature develops in direct response to strong diabatic forcing associated with sustained surface latent and sensible heating near the Gulf Stream frontal zone south of the main circulation center. Due to the nonlinear advection of the frontal feature during this time period, the previously quasi-stationary circulation center drifts eastward (and away) from the thermal forcing associated with the large SST gradients found to the west. This eastward frontal propagation acts to decrease the magnitude of the low level horizontal air temperature gradient near the center of circulation throughout the 24–42 h development period. During the 42–48 h period, the relatively quick moving frontal feature acts to severely shear the nearly stationary center of circulation in the east–west direction. As a result, the mesoscale system begins to fill during the final 6 h of integration. In addition to the control simulation, additional sensitivity experiments were conducted. These experiments were specifically designed to: (1) investigate how the magnitude of the Gulf Stream SST gradients affect the timing and degree of cyclonic development; (2) address the impact surface moisture fluxes and moist convection each have on the simulated low level mesocyclogenesis; (3) isolate the role surface sensible heating plays in the overall development of the simulated mesocyclone. Results from the SST gradient experiment indicate that a moderate enhancement of the SST distribution significantly affects the timing of the initial cyclogenesis and the maximum intensity of the simulated frontal circulation. For the "no turbulent heat flux" experiment, it appears that the elimination of surface sensible heating does not radically alter the overall structure of the simulated mesocyclone. However, the rate of development during the early stage of cyclogenesis, the absolute peak intensity of the system as well as the vertical depth of the simulated mesoscale frontal feature were all noticeably reduced when compared with the control simulation. The initial development of a closed low level circulation was delayed by nearly 18 h in the absence surface latent heat fluxes. Once formed, the system intensified throughout the 48-h period of integration, but unlike the control experiment, a mesoscale frontal feature south of the main circulation center *was not simulated*. Results from the "no surface moisture flux/no moist convection" simulation illustrate that moist convective processes play a dominant role in the overall development of the mesoscale cyclone. For this particular case, a weak and extremely shallow circulation was simulated after 24 h. This circulation quickly eroded however, and was virtually non-existent for integration times greater than 39 h.

* Corresponding author.

1. Introduction

Winter coastal cyclogenesis is a rather common occurrence in the eastern United States. The mid-Atlantic region encompassing coastal Virginia, and both North and South Carolina has been shown to be a preferred region for east coast cyclogenesis. A major reason for this high frequency is the presence of low-level diabatic heating associated with the Gulf Stream current just offshore (Sanders, 1986; Sanders and Gyakum, 1980; Colucci, 1976; Pettersen, 1956). During the winter months, cold and dry continental air contrasts sharply with the offshore maritime environment. As the continental air interacts with the warm Gulf Stream sea surface temperatures (SST), large values of surface sensible and latent heat fluxes occur (Vukovich, 1991; Wayland and Raman, 1989; Raman and Riordan, 1988). This strong and often persistent low-level diabatic forcing acts to destabilize, warm and moisten much of the marine atmospheric boundary layer (MABL) within the mid-Atlantic Gulf Stream locale (GSL). This cold air outbreak (CAO), or "atmospheric preconditioning period" can have significant implications with regard to future regional cyclogenesis. In fact, a recent study by Cione et al. (1993) has shown that if a pre-existing cyclone advects into the recently CAO-modified GSL, the potential for cyclogenic re-development at low levels significantly increases. Other studies have also shown that mesoscale sea surface temperature (SST) patterns present in and around the highly baroclinic mid-Atlantic Gulf Stream region can significantly affect, and in some instances trigger low level cyclogenesis within the GSL (Holt and Raman, 1990; Warner et al., 1990; Sanders and Gyakum, 1980). This SST-induced mesocyclogenesis may often go undetected due to the small horizontal and vertical scales initially involved. In order to better understand the dynamics of these incipient mesoscale cyclonic vortices (which most likely form near strong SST gradients), a numerical study was conducted. A major goal of this research is to investigate the evolution and physical processes associated with this type of low level mesoscale cyclogenesis. It is also of interest to investigate how changes in the SST gradient pattern potentially impact the rate and degree of cyclonic development.

2. Model description and initial conditions

In this study, the process of diabatically-induced surface mesocyclogenesis is simulated using a three-dimensional numerical model developed at North Carolina State University (Huang and Raman, 1991a; Huang, 1990). This primitive equation model is hydrostatic and anelastic in $\sigma - z$ terrain-following coordinates. The atmospheric boundary layer in this model is partitioned into the surface and the transition layer. The similarity stability functions given by Businger et al. (1971) are used to account for turbulent transport in the surface layer while a prognostic turbulent kinetic energy (TKE) equation is used above the surface layer. A turbulence closure scheme (based on TKE and turbulent energy dissipation) is used following the 2.5 level formulation of Mellor and Yamada (1982) to determine eddy diffusivity (Huang and Raman, 1991a). Subgrid scale moist convection in the model is parameterized using a variation of Kuo's (1974) scheme while a Mahrer and Pielke (1977) radiation routine incorporates the effects of radiative transfer. A modified version of the Warming-Kutler-Lomax (WKL) advection scheme (Huang and Raman, 1991a; Warming et al., 1973) is used in the horizontal while quadratic upstream interpolation is implemented in the vertical. All vertical diffusion terms are computed via a time-implicit scheme that allows the model to use a time step which is not constrained by vertical diffusion. A linear filter with a low pass property (Shapiro, 1971) is also employed. The filter is applied to the model prognostic variables at interior grid points at each time step. An additional smoother is employed in the horizontal which enhances lateral mixing of the model variables and increases the absorption of short wave disturbances in the divergent flow (Pielke, 1984).

The mesoscale model is initialized using a 1D PBL model which solves the Ekman-gradient wind equations for flow over a flat surface. During the model integration, ground temperature is set equal to the surface layer air temperature at a height of 50 m, while the SSTs are held constant throughout integration. For all simulations, zero gradient conditions are imposed at the lateral boundaries (an Orlanski-type radiation condition was tested but found to produce artificial thermal gradients at the oceanic boundaries where wave speeds are not easily determined). To minimize the thermal

gradients that are generated due to the imposed boundary conditions, a first-order upstream scheme is applied at grid points adjacent to the lateral boundaries. At the upper boundary, a radiation boundary condition (Klemp and Durran, 1983) is used to allow for the outward propagation of wave energy.

In this study, the NCSU mesoscale model is initialized with quiescent wind conditions, horizontally homogeneous temperature and moisture fields, and a uniform surface pressure of 1000 mb. For all cases simulated, the initial sounding is taken from Cape Hatteras, North Carolina on 12Z 10 January 1985, approximately 36 h after the onset of a strong CAO event. The Cape Hatteras profile is assumed to incorporate the effects of airmass modification from the recent offshore cold advective period. The model horizontal domain includes 47×34 grid points with a uniform grid interval of 20 km. In the vertical, a nineteen layer stretched grid up to 10.8 km is used. Seven of the 19 vertical levels are set below 1 km in order to establish a reasonable degree of vertical resolution within the MABL. The geographic distribution of the area of interest is presented in Fig. 1. The actual model domain incorporates much of the highly baroclinic mid-Atlantic Gulf Stream coastal region between the latitudes of 30°N and 38°N. Fig. 2 depicts contours of the idealized SST distribution used in this study and delineates the region where SST gradients are largest. For this research, the eastern boundary of the maximum SST gradient zone corresponds to the Gulf Stream front (GSF), which is also illustrated in Fig. 2. From this figure, we see that the SST contours are closely aligned with the shape of the coastline throughout much of the southern portion of the model domain. To the north, the SST isolines orient themselves in an east–west fashion as the Gulf Stream flows eastward. For the simulations conducted in this study, the magnitude of the SST's range between 5°C (278 K) near the coast and 23°C (296 K) east of the GSF.

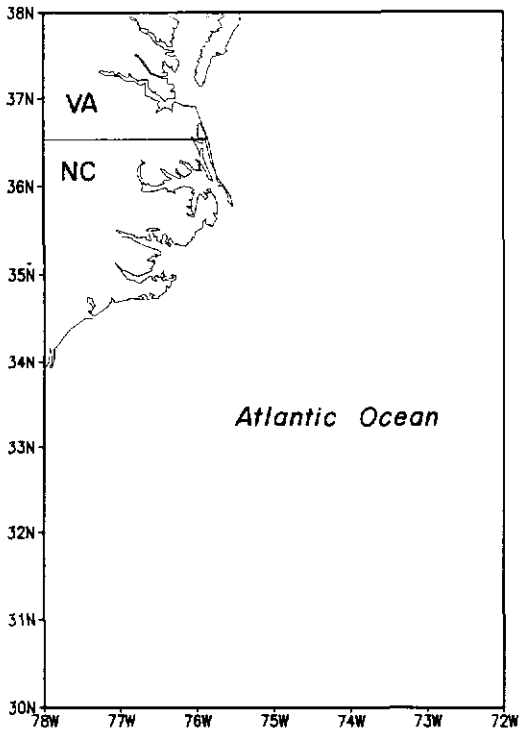

Fig. 1. Geographic representation of the highly baroclinic mid-Atlantic coastal zone between 30°N and 38°N. The idealized model domain implemented in this study approximates this region.

3. Numerical experiments and results

In the control experiment, a surface-forced mesocyclone was simulated. It is a primary goal of this research to investigate the life cycle of this system. In addition, four sensitivity simulations based on the control experiment were also conducted. The first sensitivity study was designed to investigate how changes in the magnitude of the SST gradient potentially affect the rate and degree of mesocyclogenesis. In this experiment, the magnitude of the SST gradient was increased 25% within the region of cyclogenesis simulated by the control experiment. Two additional experiments were designed to address the role moisture plays in the surface-induced mesocyclogenesis. One experiment eliminated surface moisture fluxes but still allowed moist convection to occur (by maintaining the initial relative humidity profile). The second simulation eliminated surface moisture fluxes *and* moist convection (by reducing all initial relative humidity values to zero). The final experiment was designed to isolate the role surface sensible heating played in the overall mesocyclogenesis. Similar to the case in which moisture fluxes were eliminated, turbulent surface sensible

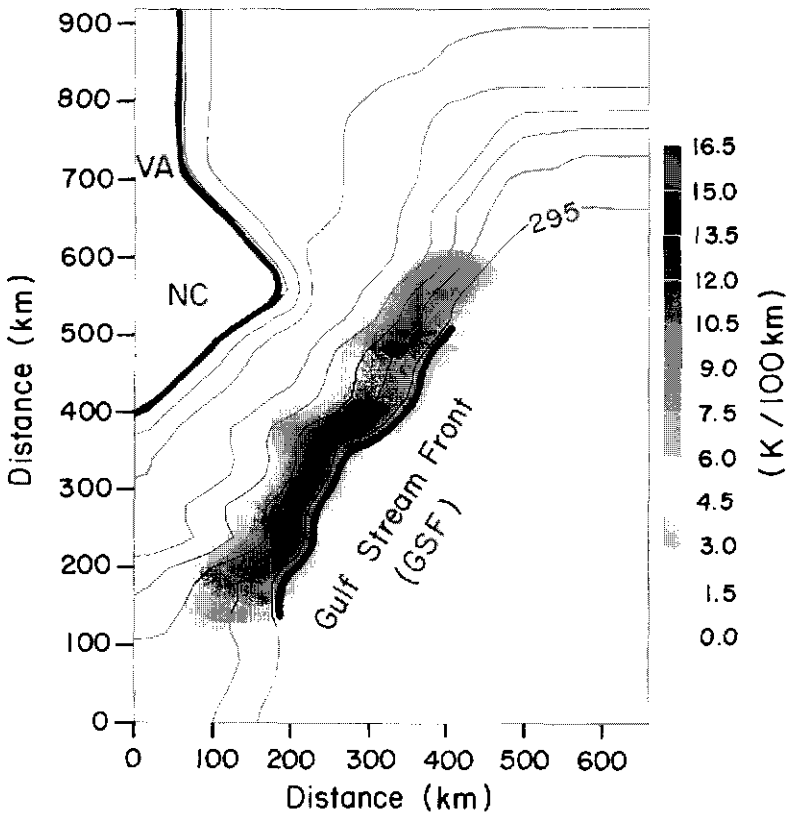

Fig. 2. The horizontal distribution of the thermal forcing at the model surface for the control cyclone superimposed over the shaded region of maximum SST gradient. Coastal land is depicted towards the northwest quadrant of the domain and has a uniform temperature of 276 K. Idealized sea surface temperatures range between 280–296 K while the maximum value of horizontal SST gradient is 15.5 K/100 km. The interval for the SST contours is 2.5 K and the SST gradient shading interval is illustrated to the right of the figure.

heating was suppressed throughout the model integration. Further discussion and results from these experiments are presented below.

3.1. Control

As described in Section 2, the initial conditions are horizontally homogeneous at each vertical level. The response within the first few hours of the control simulation is a low-level acceleration away from land towards the relatively warm shelf waters just offshore. Near surface streamline analysis at this early stage also indicates convergent flow further to the east in the vicinity of the western boundary of the idealized Gulf Stream (not shown). After 12 hours, the land warms sufficiently (relative to the adjacent coastal waters) causing a convergent pattern towards the coastal interior. At this time, a second thermally-induced convergence zone is situated near the "central region" of maximum SST gradients associated with the idealized GSF (see Figs. 2, 3a, 4a). It should be noted that this surface mesocyclogenesis occurs along a meander in the prescribed SST distribution within the vicinity of the idealized GSF. This is illustrated in Fig. 2 where a noticeable change in orientation of the 295 K isotherm is noted. It has recently been suggested that local meanders of the Gulf Stream may act to enhance the development of low level mesoscale cyclonic vortices (Reddy and Raman, 1994). From Fig. 3a, we see that the center of low

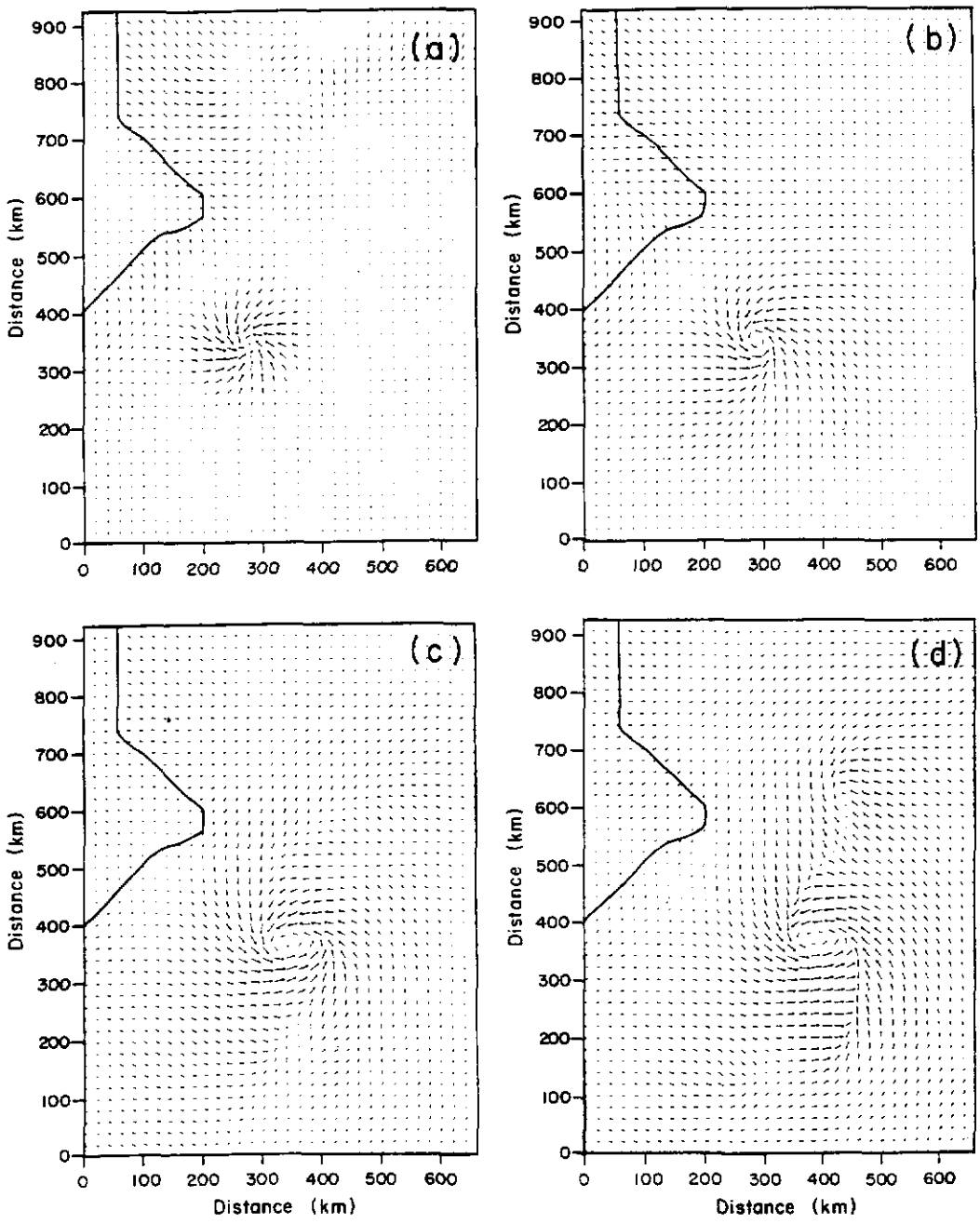

Fig. 3. The near-surface wind vector analysis for the simulated control mesocyclone. Maximum surface wind speeds are given in parenthesis. (a) The developing offshore convergence zone 12 h into the simulation (3.8 m s^{-1}). (b) The symmetrically-oriented mesovortex at 24 h (16.3 m s^{-1}). (c) The main circulation center and developing frontal feature present 36 h into the simulation (18.3 m s^{-1}). (d) The simulated mesocyclone at 48 h (19.6 m s^{-1}).

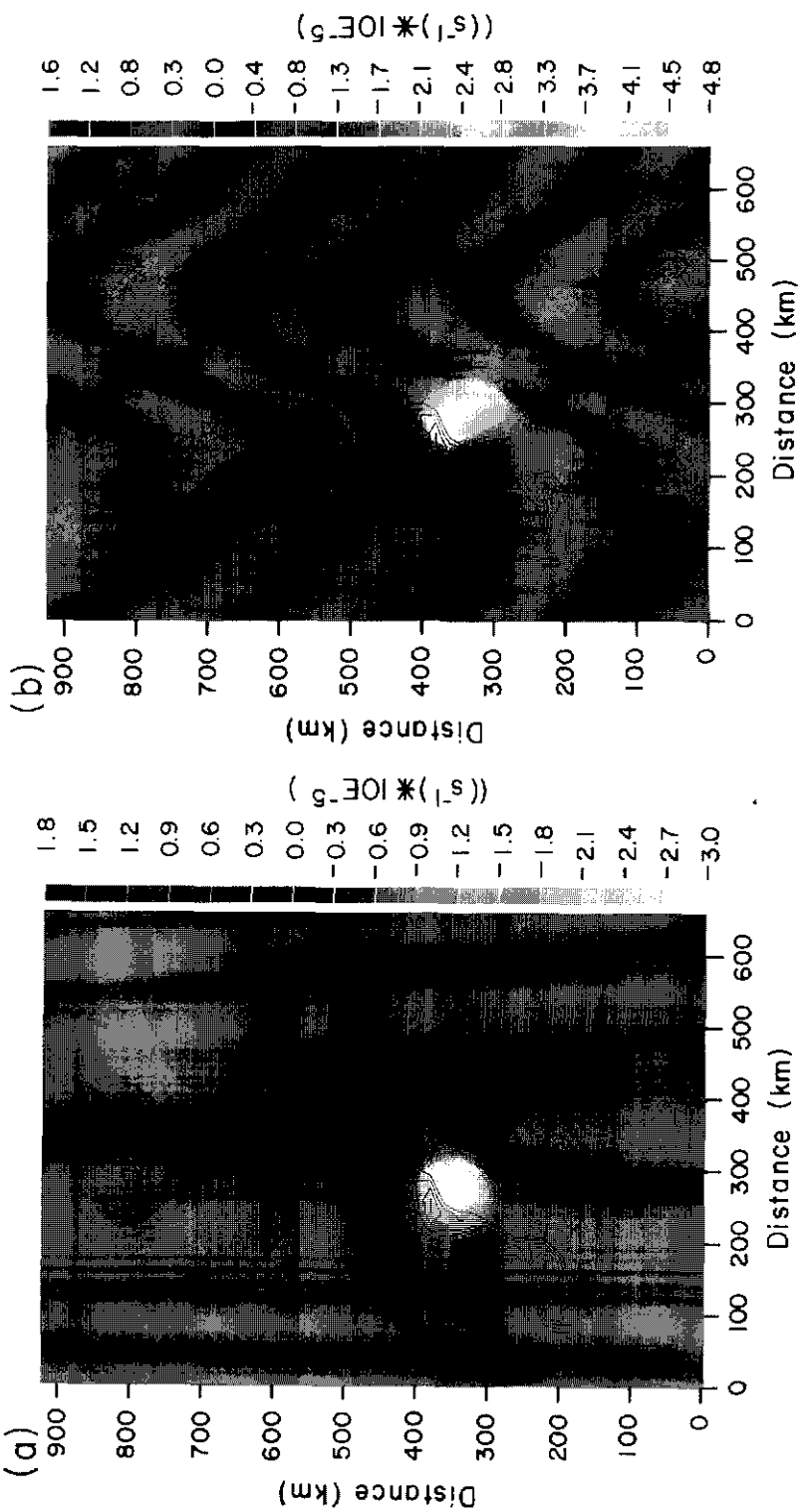
(a)
(b)
Distance (km)
Distance (km)
0
100
200
300
400
500
600
700
800
900
1.8
1.5
1.2
0.9
0.6
0.3
0.0
-0.3
-0.6
-0.9
-1.2
-1.5
-1.8
-2.1
-2.4
-2.7
-3.0
1.6
1.2
0.8
0.3
0.0
-0.4
-0.8
-1.3
-1.7
-2.1
-2.4
-2.8
-3.3
-3.7
-4.1
-4.5
-4.8

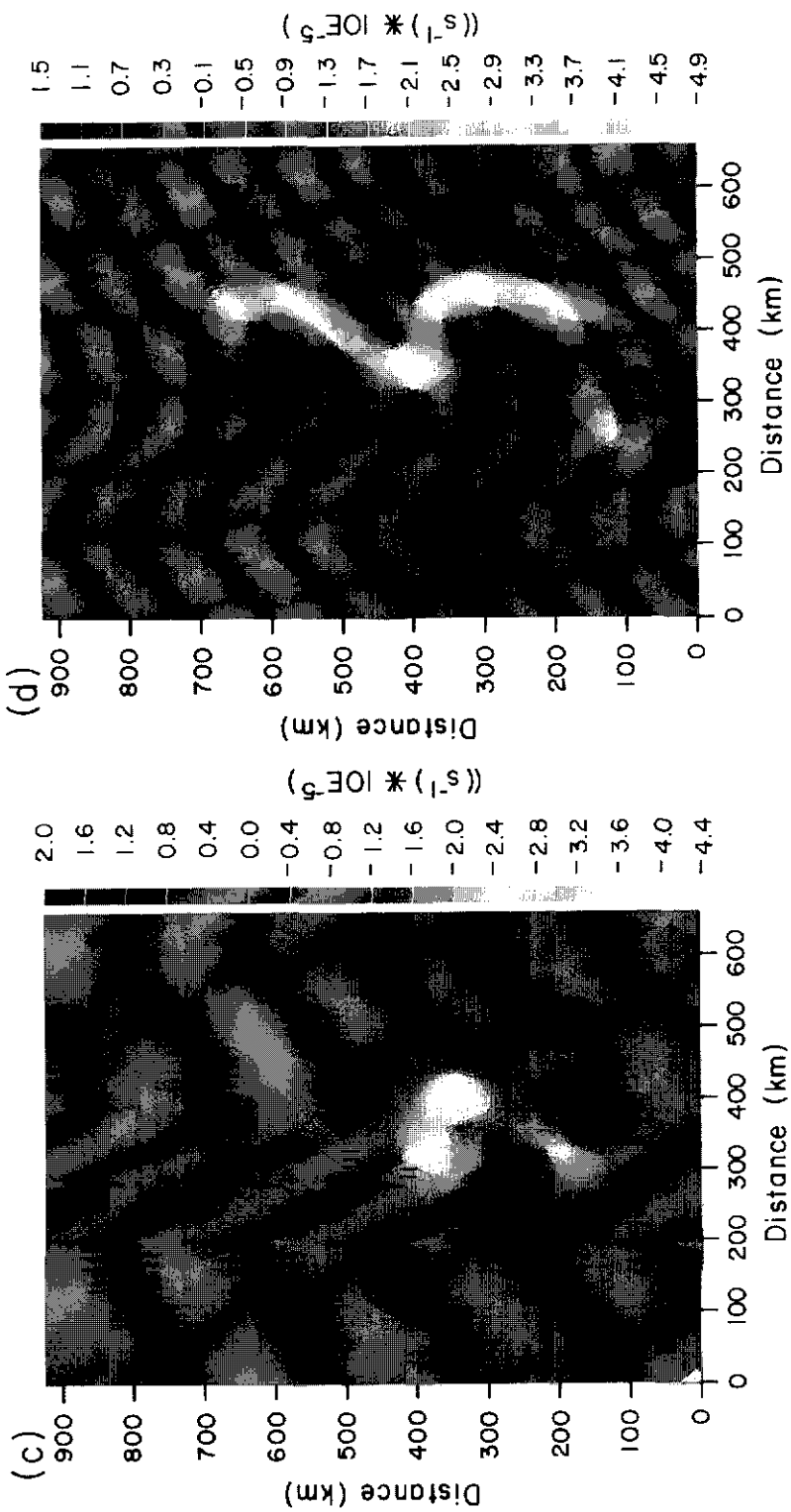

Fig. 4. The shaded near-surface (10 m) divergence field and contours of maximum SST gradient, valid for the control simulation at (a) 12 h, (b) 24 h, (c) 36 h and (d) 48 h. Note the secondary convergence zone associated with the "northern zone" of maximum SST gradient depicted in (d). The units of divergence and SST gradient are 1×10^{-5} s^{-1} and K/100 km, respectively. The SST gradient contour interval is 1 K/100 km while the shaded divergence interval is illustrated to the right of the figure.

level convergence 12 h into the simulation is co located with the central zone of maximum SST gradient.

By $t = 24$ h, the convergence center illustrated in Figs. 3a, 4a has developed significantly. Central pressure is now 997.7 mb, a decrease of 4.6 mb over the previous nine hours. Maximum wind speeds exceed 16 m s^{-1}, as the radial extent of the surface-induced system has increased to over 180 km (Fig. 3b). From Fig. 4b, we see a convergent pattern developing south of the mesovortex, eastward of the strong SST gradients. Diabatic forcing associated with turbulent heat flux transfer from the sea surface to the MABL is most likely the primary physical mechanism responsible for the simulated low level frontal convergence pattern depicted in Fig. 4b. Contours of surface sensible heating valid at this time are presented in Fig. 5. South of the main circulation center, the northeast–southwest oriented axis of alignment is roughly centered *between* the zone of

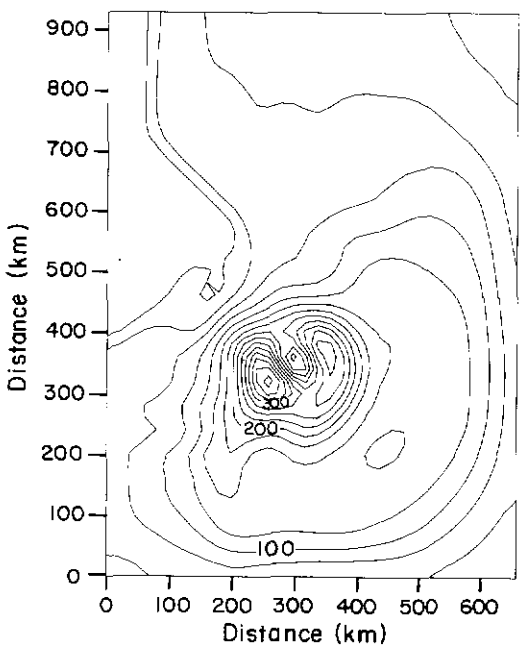

Fig. 5. Surface turbulent sensible heat transfer valid 24 h into the control simulation. South of the main vortex, within the incipient zone of frontogenesis between 150 km–275 km, average surface sensible heating is simulated to be 196 W/m^{-2}. The contour interval is 25 W/m^{-2} with a maximum contour value of 375 W/m^{-2}.

strongest SST gradients and the developing frontal feature. Similar results are evident in the surface latent heat flux distribution (not shown). After 36 h, the eastward-propagating low-level frontal feature has strengthened and is more "horizontally confined" at this time (Fig. 4c). A vertical cross section through $y = 200$ km at $t = 36$ h illustrates both the intensity and the vertical extent of the simulated frontal feature (Fig. 6). We see that the frontal circulation is confined below 1.5 km and that conditions west (east) of the 50 km convergence zone are relatively stable (unstable) at low levels.

As the intensification of the mesovortex continues from 24 to 42 h, we observe a general decreasing trend in the magnitude of the near surface horizontal air temperature gradient (see Figs. 7a, b). This most likely occurs in response to the persistent non-linear advection of the surface low eastward, or away from, the strong SST gradients associated with the prescribed Gulf Stream frontal zone. Fig. 4c (36 h) and Fig. 4d (48 h) clearly illustrate this trend. From these figures, we see that the developing frontal feature advects eastward at a rate of 2.5 m s^{-1} during the 12-h period between 36–48 h. The center of circulation, however, drifts east–northeast at a speed of less than 1 m s^{-1} during this same period. This differential rate of horizontal advection acts to severely shear the system in an east–west direction during the 42–48 h period (Fig. 3d). As a direct result, the simulated mesocyclone weakens during the last six hours of model integration time.

3.2. Sensitivity to sea surface temperature gradients

One of the sensitivity experiments conducted was the increased SST gradient case. In this simulation, the SST gradient near the initial zone of mesocyclogenesis (between 300–460 km north) was uniformly increased (refer to Fig. 2). Here, the GSF (defined as the 23°C (296 K) SST isoline) was shifted 40 km westward between 300–460 km north. As a result, the SST gradient was increased 25% within this localized region.

The mesovortex simulated under enhanced gradient conditions develops more quickly relative to the control experiment. After 18 h of integration, this vortex exhibited a sea level pressure 1 mb deeper, a near-surface relative vorticity value 43% greater and a maximum surface wind speed

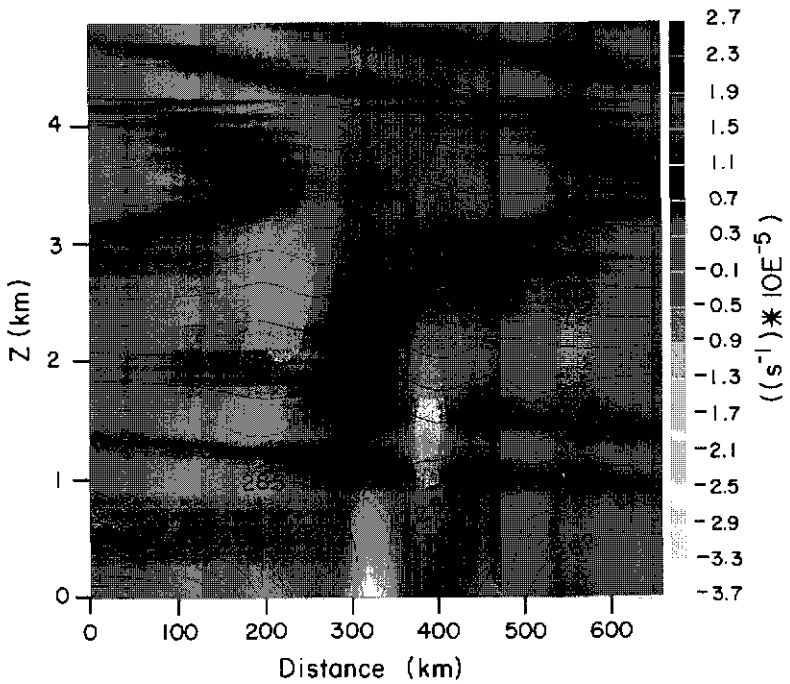

Fig. 6. A horizontal cross section of potential temperature (K) and divergence (shaded) through the developing frontal feature south of the main circulation center. The transect is taken through 200 km north and is valid 36 h into the control experiment. The units of divergence are 1×10^{-5} s^{-1}. The potential temperature contour interval is 1.5 K. Shaded divergence intervals are presented to the right of the figure.

2.7 m/s stronger than the 18-h control vortex. The time evolution of both the control and enhanced gradient simulations are presented in Tables 1 and 2, respectively. From these tables, we also see that average surface latent heat flux values associated with the developing mesoscale frontal feature south of the main circulation center are significantly higher for the increased SST gradient case

Table 1. *Time evolution of the control mesocyclone*

Hour	SLP (mb)	Vort (s^{-1})	FF ($m\,s^{-1}$)	LH $(W\,m^{-2})_{front}$
12	1002.6	0.78×10^{-5}	3.75	—
18	1000.4	3.56×10^{-5}	9.98	—
24	997.7	7.19×10^{-5}	16.30	397
30	996.2	8.11×10^{-5}	17.50	400
36	995.4	8.13×10^{-5}	18.30	406
42	993.4	8.29×10^{-5}	19.80	546
48	994.0	7.84×10^{-5}	19.60	600

The respective columns represent minimum sea level pressure (SLP) for the control mesocyclone, surface relative vorticity (Vort) for the control mesocyclone, maximum near-surface wind speed (FF) for the developing system and the area-averaged turbulent surface latent heat flux (LH) west of the simulated frontal feature. The units used are illustrated in the body of the table.

Table 2. *Time evolution of the increased SST gradient simulation relative to the control mesocyclone*

Hour	ΔSLP (mb)	ΔVor (s^{-1})	ΔFF ($m\,s^{-1}$)	ΔLH $(W\,m^{-2})_{front}$ (% change)
12	−0.45	3.2×10^{-6}	1.1	—
18	−1.02	15.4×10^{-6}	2.7	—
24	−0.84	8.9×10^{-6}	0.2	18 (+4.5%)
30	−0.68	1.8×10^{-6}	0.3	0 —
36	−0.67	2.4×10^{-6}	0.2	110 (+27.1%)
42	0.42	3.9×10^{-6}	0.0	73 (+13.4%)
48	−0.06	-3.7×10^{-6}	−0.8	−23 (−3.8%)

Column variables are defined as in Table 1. Here, however, the *difference* between the control experiment and the enhanced SST gradient simulation are presented.

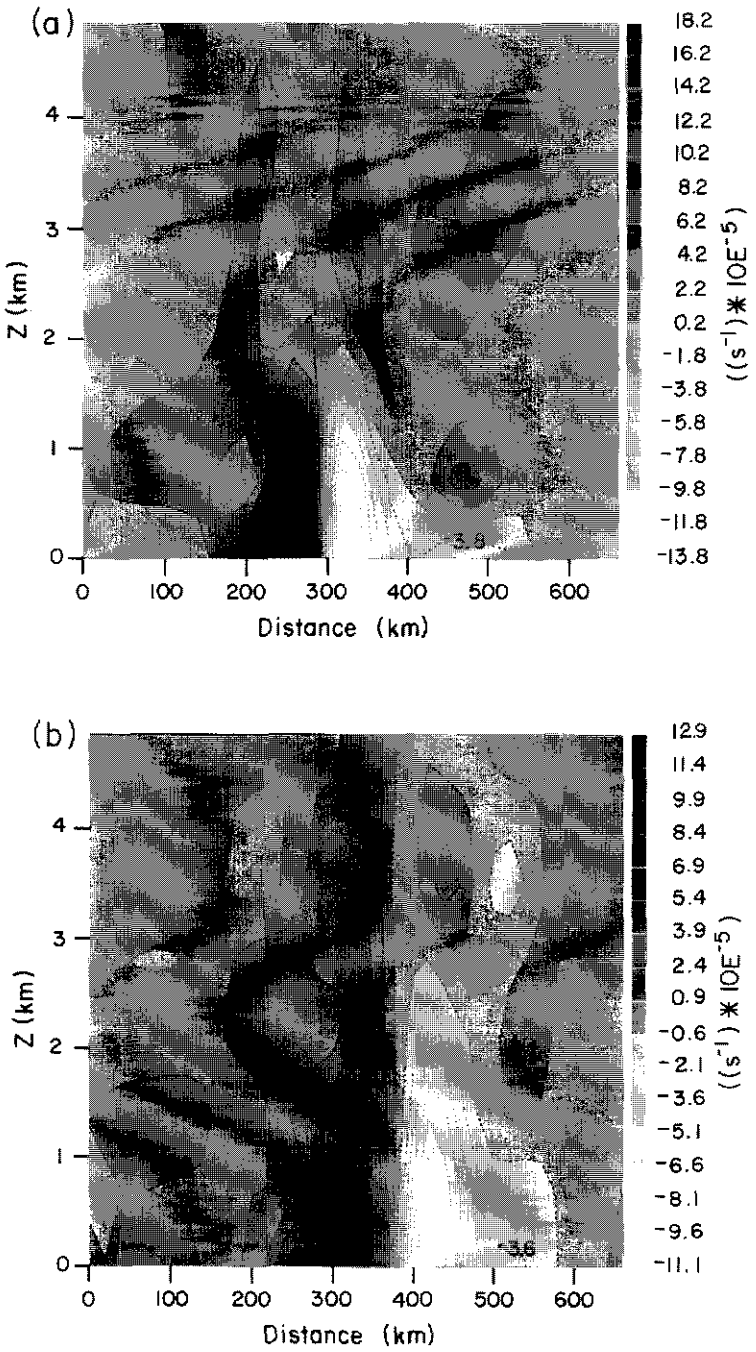

Fig. 7. A vertical cross section of the horizontal air temperature gradient (K/100 km) through the control mesovortex's center of circulation at (a) 24 h and (b) 42 h. The maximum low level SST gradient illustrated in (b) (12.9 K/100 km) is 71% of the 18.2 K/100 km depicted in (a). The shaded SST gradient contour interval for (a) is 2.0 K/100 km and 1.5 K/100 km for (b).

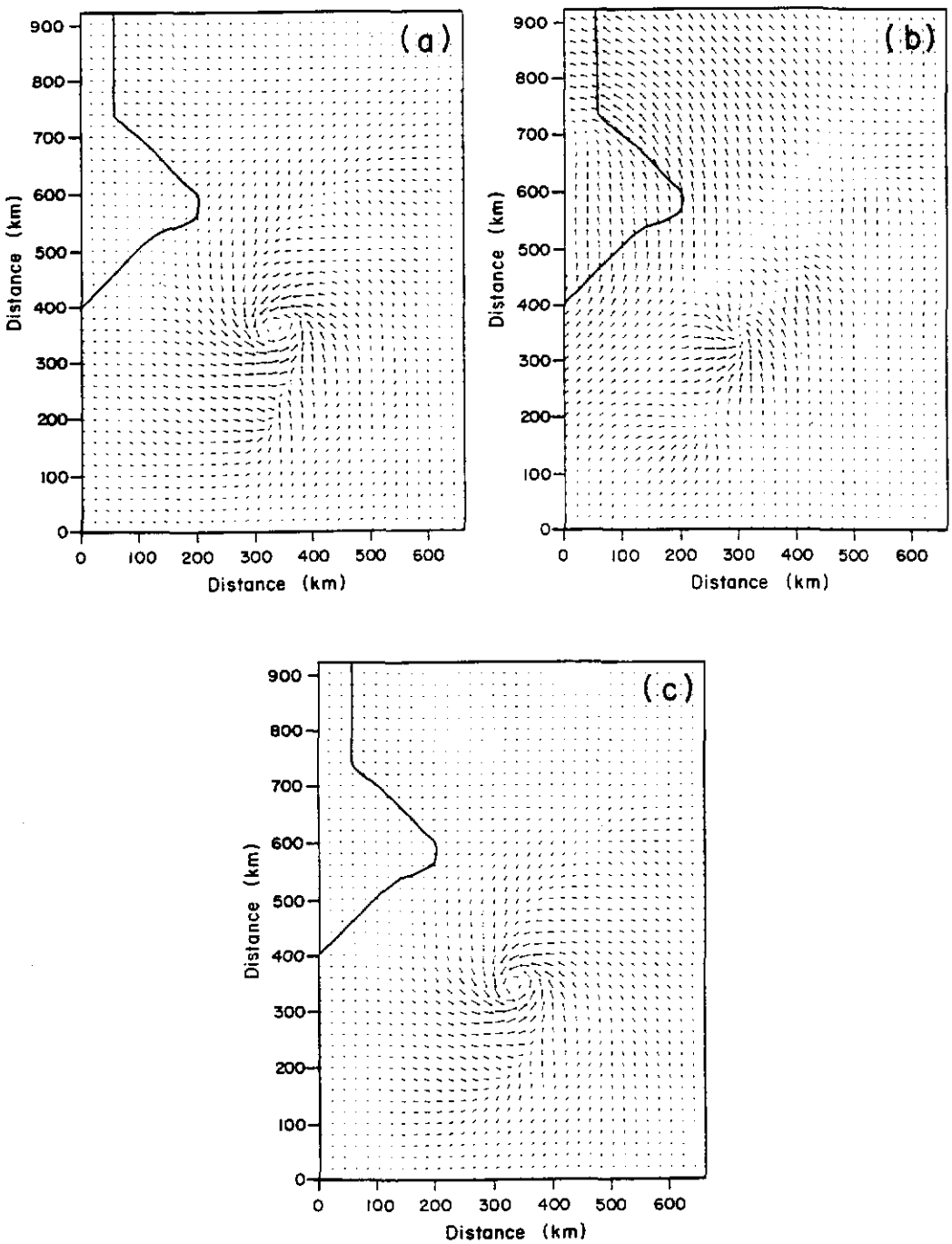

Fig. 8. The near-surface wind vector analysis valid at 36 h for (a) the increased SST gradient simulation, (b) the "no surface latent flux" experiment and (c) the "no surface sensible heat flux" simulation. Maximum surface wind speed vectors for (a), (b) and (c) are 18.5 m s^{-1}, 7.4 m s^{-1} and 17.4 m s^{-1}, respectively.

during the 36–42 h time period. It should also be noted that similar trends for surface turbulent heat flux were also found but are not presented. An inter-comparison of the surface wind speed vectors at 36 h for both the control (Fig. 3c) and the enhanced gradient case (Fig. 8a) qualitatively illustrate a more well-defined low-level convergence pattern associated with the enhanced SST simulation. Figs. 4c and 9, which depict 36-h near-surface divergence fields for the control and gradient cases, respectively, show this point more quantitatively. From Fig. 9, we see a relatively stronger and "more continuous" near-surface convergence pattern within the vicinity of the developing mesoscale frontal feature. A cross-sectional analysis of potential temperature and divergence through this convergence zone at $y = 200$ km depicts a much more vigorous frontal circulation relative to the control experiment at this time (compare Figs. 6, 10). For the enhanced SST gradient case, maximum surface convergence is simulated to be two times greater than that simulated in the control run. In addition, the simulated frontal feature is significantly deeper relative to the control case at this same time (i.e., 2.1 km versus 1.3 km).

3.3. *The impact of turbulent heat transfer*

The impact boundary layer surface fluxes have on the development of the simulated mesocyclone are of great interest. In this section we shall specifically address the rôle surface turbulent heat flux has on the simulated mesocyclogenesis. For this experiment, surface turbulent heat flux was

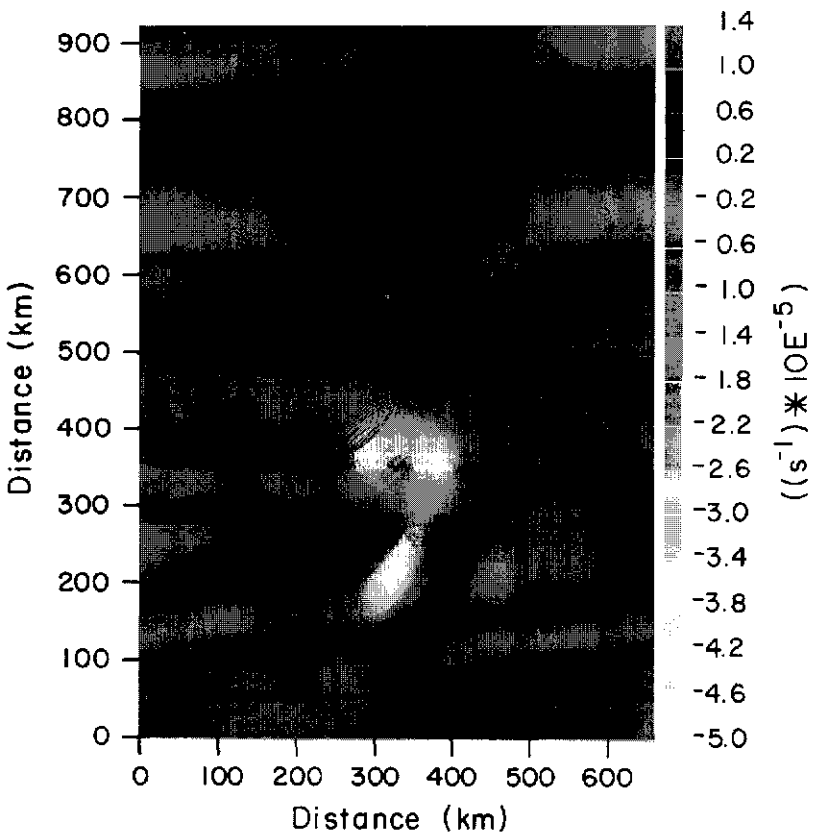

Fig. 9. The shaded near-surface (10 m) divergence field and contours of maximum SST gradient, valid for the increased SST gradient simulation at 36 h. The SST gradient contour interval is 1 K/100 km while the shaded divergence interval is illustrated to the right of the figure.

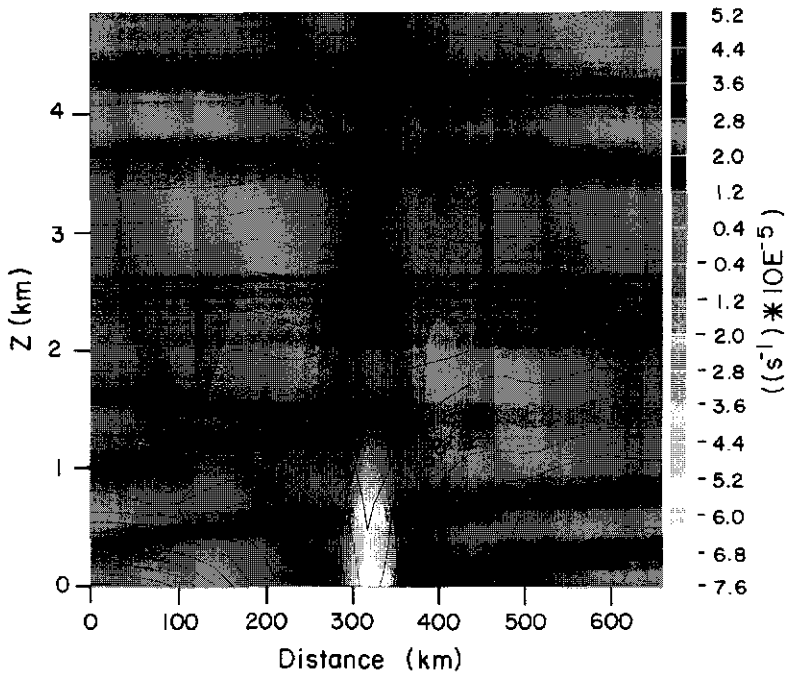

Fig. 10. The near-surface wind vector analysis valid at 36 h for the increased SST gradient simulation. Maximum low-level convergence associated with the frontal feature is simulated to be 7.6×10^{-5} s^{-1} versus 3.7×10^{-5} s^{-1} for the control at this time. The potential temperature contour interval is 1.5 K. Shaded divergence intervals are presented to the right of the figure.

deliberately suppressed throughout the 48-h time period of integration. Other than this, initial conditions remained identical to that of the control experiment. Table 3 shows the time evolution of the mesocyclone in the absence of sensible heat flux and illustrates deviations relative to the control experiment. From Table 3, we see that the elimination of surface turbulent heat transfer has the effect of suppressing the mesocyclone in terms of minimum sea level pressure. This affect is most noticeable during the rapid spin-up phase of development between 12 and 24 h. During this time period, the sea-level pressure difference (between the sensitivity experiment and the control) increases most rapidly, from 0.38 mb to 2.36 mb. Similar (negative) trends are also simulated with the vorticity and surface wind speed during this time period. Relative to the control simulation at 18 h, sea level pressure is 2.4 mb higher and surface wind speed and relative vorticity are both reduced by 20%. These results suggest that turbulent heat transfer affects the simulated mesocyclogenesis most notably during the early stages of development. Between 24 and 42 h, we see little evidence of continued deviation from the control in either the surface pressure or surface wind speed fields. That is, the *rate* of intensification during this period appears to follow that

Table 3. *Time evolution of the no sensible heat simulation relative to the control mesocyclone*

Hour	ΔSLP (mb)	ΔVor (s^{-1})	ΔFF ($m\,s^{-1}$)	ΔLH ($W\,m^{-2}$)$_{front}$ (% change)
12	0.38	-0.3×10^{-6}	0.35	—
18	1.83	-7.9×10^{-6}	−1.78	—
24	2.36	-6.8×10^{-6}	−1.60	−31 (−5.8%)
30	2.67	-1.4×10^{-6}	−1.20	−19 (−4.8%)
36	2.24	5.8×10^{-6}	−0.90	65 (+16.0%)
42	2.53	1.1×10^{-6}	−1.20	30 (+5.5%)
48	4.21	-1.7×10^{-6}	−1.00	−73 (−12.2%)

Column variables are defined as in Table 1. Here, however, the *difference* between the control experiment and the no sensible heat flux simulation are presented.

of the control, despite the elimination of surface turbulent heat transfer.

Fig. 8c illustrates the "no sensible heat flux" surface mesocyclone at $t = 36$ h. Similar to the control cyclone at this time, we see a developing convergence pattern south of the main circulation center (refer to Fig. 3c). Fig. 11 depicts the near-surface convergence at this time in relation to the maximum SST gradients. A vertical cross-section through $y = 200$ km more clearly illustrates the nature of this frontal circulation (Fig. 12). We see that the frontal feature is confined to a depth of 1 km and exhibits a maximum surface convergence of $2.9 \times 10^{-5}\ s^{-1}$. Relative to the control simulation, the depth of the circulation and the maximum near-surface convergence have been reduced by factors of 23% and 21%, respectively. It is also apparent from this figure that under conditions where the sensible heat fluxes are absent, the low-level environment west of the simulated frontal zone is considerably cooler and more stable relative to the control case. From Table 3, we see a positive deviation from the control with regard to the latent heat flux associated with the frontal feature during the 36–42-h period. Due to relatively drier conditions simulated in the absence of sensible heat fluxes, the *gradient* of near surface moisture and total latent heat flux were simulated to be greater, *despite* weaker wind conditions present at low levels near the mesoscale frontal zone.

3.4. *Affects of moisture*

The final two sensitivity simulations conducted were designed to investigate the role moisture played in the simulated mesocyclogenesis. One

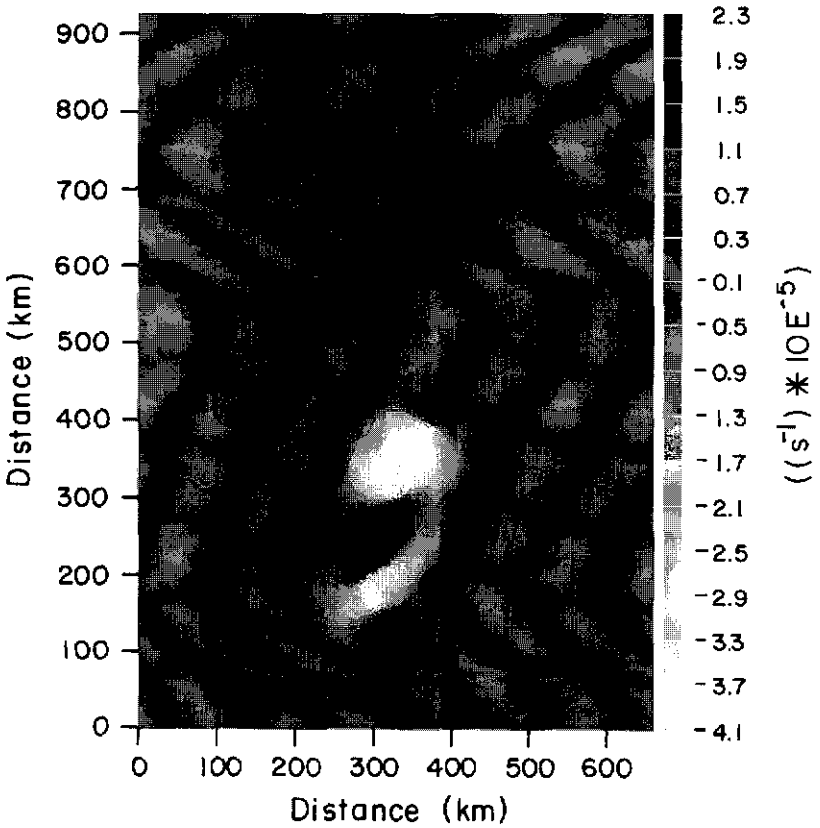

Fig. 11. The shaded near-surface (10 m) divergence field and contours of maximum SST gradient, valid for the "no surface sensible heat flux" simulation at 36 h. The SST gradient contour interval is 1 K/100 km while the shaded divergence interval is illustrated to the right of the figure.

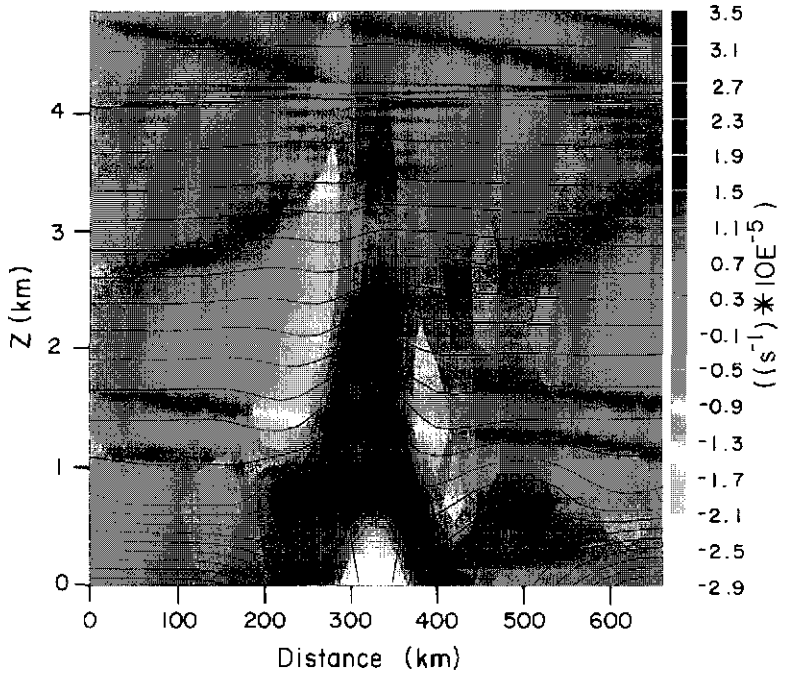

Fig. 12. The near-surface wind vector analysis valid at 36 h for the "no surface sensible heat flux" simulation. Maximum simulated low level convergence through the frontal feature is 2.9×10^{-5} s^{-1} or 78% of the control at this time. The potential temperature contour interval is 1.5 K. Shaded divergence intervals are presented to the right of the figure.

of the two experiments eliminated surface latent heat fluxes throughout the 48-h simulation period. Similar to the case which suppressed surface sensible heating, all other initial conditions were identical to that of the control experiment. The second experiment also eliminated surface moisture fluxes but in addition, also suppressed moist convection from occurring by setting all initial relative humidity values to zero. These two experiments were designed to help elucidate the relative importance surface moisture fluxes and moist convection each have on the simulated mesocyclogenesis.

In the absence of latent heat fluxes, the onset of the mesocyclogenesis is delayed by roughly 18 h, occurring at $t = 30$ h (compared to $t = 12$ h for the control experiment). For this particular simulation, the location of the initial cyclogenesis corresponds closely to where the control cyclogenesis occurs (compare Fig. 13 with Fig. 4a). Fig. 8b illustrates the simulated surface wind speed vectors, valid at $t = 36$ h. Table 4 depicts the time evolution of the surface wind speed and relative vorticity for the case where latent heat fluxes are suppressed. In addition, deviations from the control experiment are presented.

From Table 4, we see that in the absence of latent heat fluxes, the mesovortex continues to *intensify throughout* the 48-h simulation period. However, unlike the previous simulations, a close qualitative resemblance to the control simulation was not observed after the initial period of mesocyclogenesis. It should also be noted that the mesofrontal feature south of the main circulation center (which was simulated in each of the three experiments previously discussed) *was not simulated* in this experiment. Nevertheless, even without surface moisture flux, a closed low level circulation forms and stengthens to roughly 55% of the control maximum intensity.

The simulation which eliminated both surface latent heat flux and moist convection was also run for 48 h. However, unlike the previous moisture sensitivity experiment, very little development

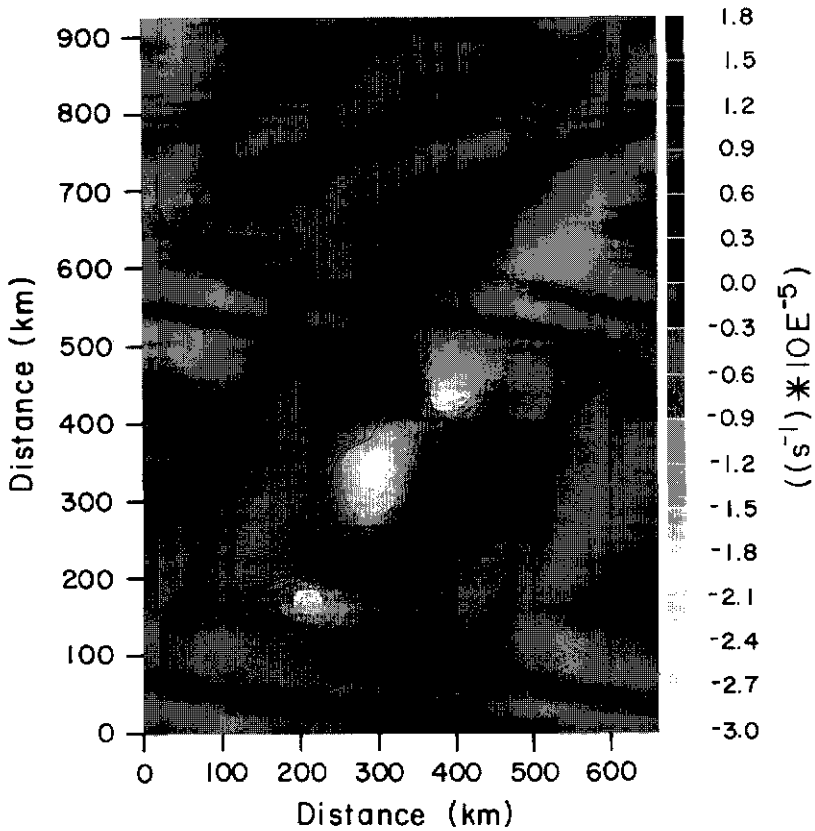

Fig. 13. The shaded near-surface (10 m) divergence field and contours of maximum SST gradient, valid for the "no surface latent heat flux" simulation at 36 h. Maximum low level convergence, east of the region of strongest SST gradient, is 3.0×10^{-5} s^{-1} at this time. The SST gradient contour interval is 1 K/100 km while the shaded divergence interval is illustrated to the right of the figure.

Table 4. *Time evolution of surface wind speed and relative vorticity for the moisture simulations relative to the control mesocyclone*

Hour	$(FF_{LH}(\Delta FF))$ m s^{-1}	$(Vor_{LH}(\Delta Vor))$ s^{-1}	$(FF_{LH/CON}(\Delta FF))$ m s^{-1}	$(Vor_{LH/CON}(\Delta Vor))$ s^{-1}
24	—	—	2.80 (−13.5)	1.08×10^{-5} (−6.11)
30	2.20 (−15.3)	0.20×10^{-5} (−7.90)	3.40 (−14.1)	1.10×10^{-5} (−7.01)
36	7.40 (−10.9)	1.95×10^{-5} (−6.18)	3.70 (−14.6)	1.13×10^{-5} (−7.00)
42	10.30 (−9.5)	3.56×10^{-5} (−4.73)	—	—
48	11.50 (−8.1)	4.18×10^{-5} (−3.66)	—	—

The respective columns represent maximum near-surface wind speed for the "no latent heat flux" mesocyclone (including the control relative deviation) ($FF_{LH}(\Delta FF)$), the maximum surface relative vorticity for the "no latent heat flux" mesocyclone (including the control relative deviation) ($Vor_{LH}(\Delta Vor)$), the maximum near-surface wind speed for the "no latent heat flux/no moist convection" mesocyclone (including the control relative deviation) ($FF_{LH/CON}(\Delta FF)$) and the maximum surface relative vorticity for the no latent heat flux/no moist convection" mesocyclone (including the control relative deviation) ($Vor_{LH/CON}(\Delta Vor)$). The units used are illustrated in the body of the table.

occurred throughout the period of model integration (see Table 4). After 24 h, a very weak and shallow (i.e., less than 200 m deep) closed circulation was simulated near the central region of maximum SST gradients. However, shortly after 36 h, the shallow surface low began to deteriorate and was virtually non-existent after 39 h. Of the 5 experiments simulated, the circulation observed in this sensitivity study was the weakest and most short lived. These results illustrate that latent heat release resulting from mesoscale convection plays a dominant role in the overall development of the simulated mesocyclone.

4. Summary

In summary, mesocyclogenesis was initiated along a Gulf Stream meander in a region where the horizontal SST gradients were maximized. Under initially calm wind conditions, a mesoscale vortex on the order of 140 km formed 12 h into the control experiment. Intensification of this mesoscale system was simulated through the 12–42 h time period. During the 24–48 h interim, a mesoscale frontal feature developed south of the main circulation center. This feature developed in response to strong and persistent diabatic forcing associated with boundary layer surface turbulent heat fluxes. The location of this mesoscale frontogenesis corresponded closely to the location of the Gulf Stream front south of the main low center. Within this region, SST gradients are of the order of 15 K/100 km were prescribed. A vertical cross section through the developing frontal feature at $t = 36$ h illustrated that the depth of the circulation was confined to 1.3 km. A potential temperature cross section at this time depicted contrasting airmasses across the simulated frontal boundary with warmer (colder) and more unstable (stable) atmospheric conditions east (west) of the low-level convergence zone. This mesoscale frontal feature strengthened throughout the period of model integration and advected eastward at an average rate of 2.5 m s^{-1}. This rate of advection was significantly greater than that of the main circulation center situated to the north. As a result, this mesoscale system became severely sheared in the east–west direction and weakened over the ensuing 42–48-h period.

Results from the increased SST gradient simulation illustrated that relatively moderate enhancements (25%) of the prescribed surface forcing significantly altered the *timing* in the initial development of the mesoscale cyclogenesis. Relative to the control experiment, the onset of initial cyclogenesis was simulated to occur several hours earlier. While the absolute intensification in this case (in terms of surface pressure) was only slightly deeper than that of the control, the stronger SST gradients associated with this experiment helped to *noticeably intensify* the magnitude of the simulated frontal feature south of the mesoscale circulation center. At $t = 36$ h, the frontal feature associated with this simulation illustrated a deeper structure (i.e., 2.1 km versus 1.3 km) and a more vigorous low-level convergence pattern (i.e., 7.6×10^{-5} s^{-1} versus 3.7×10^{-5} s^{-1}). Average surface latent heat fluxes associated with the developing mesoscale frontal feature under enhanced SST gradient conditions were 27% greater when compared to control values simulated at 36 h.

Results from the experiment, in which sensible heat fluxes were removed, illustrated that surface turbulent heat transfer impacted the development of the mesocyclone most notably during the rapid, "spin-up" stage of development. 18 h into this simulation, sea-level pressure was 2.4 mb higher and surface wind speed and relative vorticity were both 20% lower than those values produced in the control experiment. However, the rate of intensification throughout the 24–42 h period of integration was very similar to that of the control experiment. In addition, the overall structure of the simulated mesocyclone in this case compared well with the control throughout the development stage. Still, the absolute intensity of the mesocyclone was somewhat reduced when turbulent sensible heat fluxes were eliminated. A cross section analysis through the developing mesoscale frontal feature 36 h into the simulation illustrated a 1.0 km deep circulation. At this time, maximum surface convergence was simulated to be 2.9×10^{-5} s^{-1}. These respective values represents 28% and 21% negative deviations from the control experiment.

In the case where surface latent heat fluxes were eliminated, the initial develoment of a cyclonically-oriented closed mesoscale circulation was delayed by approximately 18 h. The incipient vortex formed after 30 h and continued to develop throughout the 48-h period of model integration. For this experiment, maximum values for surface wind speed and relative vorticity were simulated to be

11.5 m s^{-1} and 4.18×10^{-5} s^{-1}, down 41% and 53%, respectively, from the control case. Similar to the control experiment, the initial region of cyclogenesis occurred within the "central region" of strongest SST gradients. However, unlike the control, no frontal feature south of the main circulation center developed during the simulation period. The delayed nature of the initial development of mesocyclogenesis in the absence of moisture flux illustrates that the vertical transport of moisture and subsequent latent heat release is an important physical mechanism responsible for lowering surface pressures (and hence low-level convergence) in and around the eventual region of mesoscale cyclogenesis. In addition, the failure to simulate a well-defined convergence pattern south of the main circulation center elucidates the critical role surface moisture fluxes play in the eventual development of the mesoscale frontal feature.

In the final experiment, both surface moisture fluxes and moist convective processes were suppressed throughout the 48-h model integration period. Under these conditions, an extremely shallow, cyclonically-oriented mesoscale circulation was simulated 24 h into the experiment. The circulation, which reached a peak surface wind speed of 3.7 m/s at 36 h, decayed rapidly and completely dissipated after 39 h. Results from the two moisture simulations illustrate the dominant role latent heat release plays in the development of the simulated mesocyclone. In the absence of surface moisture fluxes, the mesoscale system still manages to intensify due to the moisture present in the initial sounding. However, when turbulent latent heat flux is eliminated *and* atmospheric moisture conditions above the surface are dry, latent heat release resulting from convective processes becomes impossible. Under these conditions, only a shallow and transient circulation was simulated. It is clear that while turbulent sensible heat transfer near the surface can result in low level warming and convective instability, it is the much larger latent heat release associated with condensation aloft that allows the atmospheric column to warm over a significantly deep layer.

5. Acknowledgments

The authors whish to thank Dr. R. P. Weglarz for several helpful discussions and for proofreading the final draft of the manuscript. Appreciation also goes to Amy Herman for her word processing assistance and Luann Salzillo for graphics support. This work was supported by the Atmospheric Sciences Division, National Science Foundation under Grant ATM 9212636. Computer resources were provided by the MCNC, Research Triangle Park and by the National Supercomputing Center for Energy and the Environment, University of Nevada, Las Vegas.

REFERENCES

Businger, J. A., Wyngaard, J. C., Izumi, Y. and Bradley, E. F. 1971. Flux profile relationship in the atmospheric surface layer. *J. Atmos. Sci.* **28**, 181–189.

Cione, J. J., Raman, S. and Pietrafesa, L. J. 1993. The effect of Gulf Stream induced baroclinicity on U.S. east coast winter cyclones. *Mon. Wea. Rev.* **121**, 421–430.

Huang, C. Y. and Raman, S. 1991a. Numerical simulation of January 28 cold air outbreak during GALE, Part I: The model and sensitivity tests of turbulence closure. *Boundary-Layer Meteorology* **55**, 381–407.

Huang, C. Y. and Raman, S. 1991b. A comparative study of advection schemes: Featuring a one-step modified WKL algorithm. *Mon. Wea. Rev.* **119**, 2900–2918.

Fantini, M. 1990. The influence of heat and moisture fluxes from the ocean on the development of baroclinic waves. *J. Atmos. Sci.* **47**, 840–855.

Klemp, J. B. and Durran, D. R. 1983. An upper boundary condition permitting internal gravity wave radiation in a numerical model. *Mon. Wea. Rev.* **111**, 430–444.

Kuo, Y. H. 1974. Further studied of the parameterization of the influence of cumulus convection on large-scale flow. *J. Atmos. Sci.* **31**, 1232–1240.

Mahrer, Y. and Pielke, R. A. 1977. The effects of topography on the sea and land breeze in a two-dimensional numerical model. *Mon. Wea. Rev.* **105**, 1151–1162.

Mellor, G. L. and Yamada, T. 1982. Development of a turbulence closure model for geophysical fluid problems. *Rev. Geophys. Space Phys.* **20**, 851–875.

Petterssen, S. 1956. *Weather analysis and forecasting*. McGraw-Hill, 428 pp.

Pielke, R. A. 1984. *Mesoscale meteorological modeling*. Academic Press, New York, 612 pp.

Raman, S. and Riordan, A. J. 1988. The Genesis of Atlantic Lows Experiment (GALE): The Planetary Boundary layer Subprogram. *Bull. Amer. Meteor. Soc.* **69**, 161–172.

Reddy, N. C. and Raman, S. 1994. Observations of a

mesoscale circulation over the Gulf Stream region. *The Global Atmosphere Ocean System* **2**, 21–39.

Sanders, F. 1986. Explosive cyclogenesis in the west-central North Atlantic Ocean, 1981–1984. Part I: Composite structure and mean behavior. *Mon. Wea. Rev.* **114**, 1781.

Sanders, F. J. and Gyakum, J. R. 1980. Synoptic-dynamic climatology of the "bomb". *Mon. Wea. Rev.* **108**, 1589–1606.

Shapiro, R. 1971. The use of linear filtering as a parameterization of atmospheric diffusion. *J. Atmos. Sci.* **28**, 523–531.

Vukovich, F. M., Dunn, J. W. and Crissman, B. W. 1991. Aspects of the evolution of the marine boundary-layer during cold air outbreaks off the south east coast of the United States. *Mon. Wea. Rev.* **119**, 2252–2278.

Warming, R. F., Kutler, P. and Lomax, H. 1973. Second and third-order non centered difference schemes for nonlinear hyperbolic equations. *AIAA J.* **11**, 189–196.

Warner, T. T., Lakhtakia, M. N., Doyle, J. D. and Pearson, R. A. 1990. Marine atmospheric boundary layer circulations forced by Gulf Stream sea surface temperature gradients. *Mon. Wea. Rev.* **118**, 309–323.

Wayland, R. and Raman, S. 1989. Mean and turbulent structure of a baroclinic marine boundary-layer during the 28 January 1986 cold air outbreak (GALE 86). *Boundary-Layer Meteor.* **48**, 227–254.